Appl. Phys. B 90, 619–628 (2008)
DOI: 10.1007/s00340-007-2925-y

Applied Physics B
Lasers and Optics

A. FAROOQ✉
J.B. JEFFRIES
R.K. HANSON

CO_2 concentration and temperature sensor for combustion gases using diode-laser absorption near 2.7 μm

High Temperature Gasdynamics Laboratory, Department of Mechanical Engineering, Stanford University, Stanford, CA 94305, USA

Received: 16 October 2007 /
Revised version: 10 December 2007
Published online: 29 January 2008 •

ABSTRACT A new tunable diode-laser sensor based on CO_2 absorption near 2.7 μm is developed for high-resolution absorption measurements of CO_2 concentration and temperature. The sensor probes the $R(28)$ and $P(70)$ transitions of the $\nu_1 + \nu_3$ combination band of CO_2 that has stronger absorption line-strengths than the bands near 1.5 μm and 2.0 μm used previously to sense CO_2 in combustion gases. The increased absorption strength of transitions in this new wavelength range provides greatly enhanced sensitivity and the potential for accurate measurements in combustion gases with short optical path lengths. Simulated high-temperature spectra are surveyed to find candidate CO_2 transitions isolated from water vapor interference. Measurements of line-strength, line position, and collisional broadening parameters are carried out for candidate CO_2 transitions in a heated static cell as a function of temperature and compared to literature values. The accuracy of a fixed-wavelength CO_2 absorption sensor is determined via measurement of known temperature and CO_2 mole fraction in a static cell and shock-tube. Absorption measurements of CO_2 are then made in a laboratory flat-flame burner and in ignition experiments of shock-heated n-heptane/O_2/argon mixtures to illustrate the potential of this sensor for combustion and reacting-flow applications.

PACS 42.62.Fi; 42.55.Px; 07.07.Df

1 Introduction

The development of diagnostics based on laser-absorption spectroscopy for combustion applications has been an important and active field of research over the past two decades, due to the advantages of this non-intrusive optical sensing technique compared to traditional sampling-based sensing methods. These tunable diode-laser (TDL) sensors have been used successfully to provide in situ, time-resolved, line-of-sight measurements of temperature, gas species concentration, velocity, density, mass flux, and pressure in a variety of combustion environments [1–5]. The information provided by such sensors can be useful in the development of modern propulsion and combustion systems, e.g. to facilitate design advancements, improve efficiency, and reduce pollutant emissions. CO_2 is an attractive target gas for hydrocarbon-fueled systems as it is a primary combustion product and its concentration can be interpreted to indicate combustion efficiency. CO_2 has absorption spectra in the near- to mid-infrared region as illustrated in Fig. 1, where the absorption line-strengths of CO_2 are plotted as a function of wavelength from 1 to 3 μm at a representative combustion temperature of 1500 K [6, 7]. Most current CO_2 absorption sensors are designed to exploit robust telecommunications diode lasers and optical fiber technology in the 1.3–1.6 μm wavelength region. Thus, previous sensors for CO_2 used the combination bands near 1.55 μm ($2\nu_1 + 2\nu_2 + \nu_3$) [8–10] and 2.0 μm ($\nu_1 + 2\nu_2 + \nu_3$) [11, 12] that are approximately 1000 and 50 times weaker (respectively) compared to the $\nu_1 + \nu_3$ and $2\nu_2 + \nu_3$ bands near 2.7 μm. The small absorption strengths of the transitions used previously have generally led to sensors with relatively long path lengths and/or required significant time averaging.

Recent developments in semiconductor diode-laser technology have extended the range of continuous-wavelength (cw) room-temperature single-mode diode lasers to

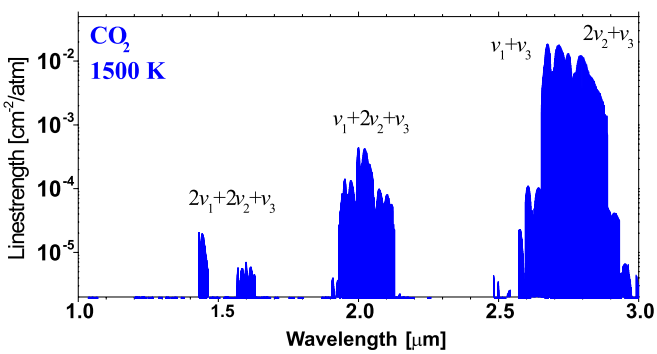

FIGURE 1 Absorption line-strengths of CO_2 at 1500 K (from HITRAN [6, 7])

✉ Fax: +1-650-723-1748, E-mail: aamir@stanford.edu

2.8 μm [13], allowing access to stronger vibrational bands of CO_2. Absorption sensors at these longer wavelengths offer greater sensitivity and potential for measurements in systems with short optical path lengths. Our current research is aimed at developing TDL absorption diagnostics for combustion applications that use CO_2 transitions near 2.7 μm; preliminary results of this work were presented earlier [14]. Candidate transitions are selected based on absorption strength and isolation from interference of neighboring transitions of CO_2/H_2O as well as from other combustion gases. For gas-temperature sensing based on the ratio of absorption in two CO_2 transitions, use of well-separated lower-state internal energies provides sensitivity of the absorption ratio to temperature. The selected CO_2 transitions $R(28)$ and $P(70)$ belong to the $\nu_1+\nu_3$ vibrational band and have lower-state energies (E'') of 316.77 and 1936.09 cm^{-1}, respectively. The two CO_2 transitions are accessed with two different lasers and a fixed-wavelength direct-absorption technique [15] is used in situations where large sensor bandwidth is required, e.g. for time-resolved measurements in shock-heated gases.

For the selected lines, fundamental spectroscopic parameters (line-strength, line position, self-broadening coefficient) are first measured in a heated static cell and compared with literature and database values. Ar-broadening parameters are also measured for these two transitions as we anticipate the use of this sensor in shock-tubes where the primary bath gas is often Ar. To our knowledge, these Ar-broadening parameters are not previously available in the literature. The accuracy of the fixed-wavelength CO_2 temperature sensor is validated in the static cell and shock-tube with CO_2–Ar mixtures.

CO_2 concentrations are then measured via absorption in the combustion region above a flat-flame burner and compared with chemical equilibrium calculations. Measurements of CO_2 and temperature are subsequently carried out behind reflected shocks in heptane–O_2 ignition experiments and the results compared with kinetic models. Taken together with our preliminary results [14], this work presents the first absorption measurements of CO_2 in a combustion environment near 2.7 μm using cw distributed-feedback (DFB) diode lasers.

2 Theory

The fundamental theory of direct-absorption spectroscopy has been detailed by numerous researchers [15, 16] and is reproduced here briefly to define our notation. The fundamental equation governing line-of-sight laser absorption spectroscopy is the Beer–Lambert relation. This equation relates the transmitted intensity I_t through a uniform gas medium of length L [cm] to the incident intensity I_0 as

$$\left(\frac{I_\mathrm{t}}{I_0}\right)_\nu = \exp(-k_\nu L)\,, \tag{1}$$

where k_ν [cm^{-1}] is the spectral absorption coefficient. For an isolated transition i,

$$k_\nu = P x_\mathrm{abs} S_i(T)\varphi_\nu\,, \tag{2}$$

where x_abs is the mole fraction of the absorbing species, $S_i(T)$ [$\mathrm{cm}^{-2}\,\mathrm{atm}^{-1}$] the line-strength of the transition, and φ_ν [cm] the line-shape function. The product $k_\nu L$ is known as the spectral absorbance α_ν:

$$\alpha_\nu \equiv -\ln\left(\frac{I_\mathrm{t}}{I_0}\right) = k_\nu L = P x_\mathrm{abs} S_i(T)\varphi_\nu L\,. \tag{3}$$

Since the line-shape function φ_ν is normalized such that $\int \varphi_\nu \,\mathrm{d}\nu \equiv 1$, the integrated absorbance can be expressed as

$$A_i = \int \alpha_\nu \,\mathrm{d}\nu = P x_\mathrm{abs} S_i(T) L\,. \tag{4}$$

The line-shape function φ_ν is usually approximated using a Voigt profile characterized by the collision-broadened full-width at half maximum (FWHM), $\Delta\nu_\mathrm{c}$ [cm^{-1}], and the Doppler FWHM, $\Delta\nu_\mathrm{d}$ [cm^{-1}]. The collisional width $\Delta\nu_\mathrm{c}$ is proportional to the system pressure in the following way:

$$\Delta\nu_\mathrm{c} = P\sum_j x_j 2\gamma_{j-\mathrm{abs}}\,. \tag{5}$$

Here, $\gamma_{j-\mathrm{abs}}$ [$\mathrm{cm}^{-1}\,\mathrm{atm}^{-1}$] is the broadening coefficient due to collisions between perturbing species j and the absorbing species. With knowledge of the temperature-dependent coefficient n, the collisional broadening coefficient γ_j can be calculated using the following scaling relation:

$$\gamma_j(T) = \gamma_j(T_0)\left(\frac{T_0}{T}\right)^n\,. \tag{6}$$

The line-strength, in units of $\mathrm{cm}^{-2}/\mathrm{atm}$, is a function of temperature:

$$S(T) = S(T_0)\frac{Q(T_0)}{Q(T)}\left(\frac{T_0}{T}\right)\exp\left[-\frac{hcE''}{k_\mathrm{B}}\left(\frac{1}{T}-\frac{1}{T_0}\right)\right] \times\left[1-\exp\left(\frac{-hc\nu_0}{k_\mathrm{B}T}\right)\right]\left[1-\exp\left(\frac{-hc\nu_0}{k_\mathrm{B}T_0}\right)\right]^{-1}\,, \tag{7}$$

where h [J s] is Planck's constant, c [cm/s] is the speed of light, k_B [J/K] is Boltzmann's constant, the partition function, $Q(T)$, of CO_2 is taken from HITRAN [17], T_0 [K] is the reference temperature (usually 296 K), ν_0 [cm^{-1}] is the line-center frequency, and E'' [cm^{-1}] is the lower-state energy of the transition. The lower-state energy E'' determines the equilibrium population fraction in the lower state as a function of temperature, and thus influences how the strength of a particular transition varies with temperature.

Diode-laser absorption measurements of temperature are commonly based on a two-line technique [9]. Temperature is inferred from the ratio of the integrated absorbance (scanned-wavelength direct absorption) or line-center absorbance (fixed-wavelength direct absorption) of two molecular transitions of the same species.

3 Line selection

Absorption spectra based on the HITRAN database [6, 7] near 2.7 μm are computed for combustion conditions (T = 1000–2000 K, P = 1 atm, L = 10 cm, 10% H_2O, 10% CO_2, balance of air) and used to find isolated CO_2 transitions. The $R(28)$ transition of CO_2's $\nu_1+\nu_3$ vibrational

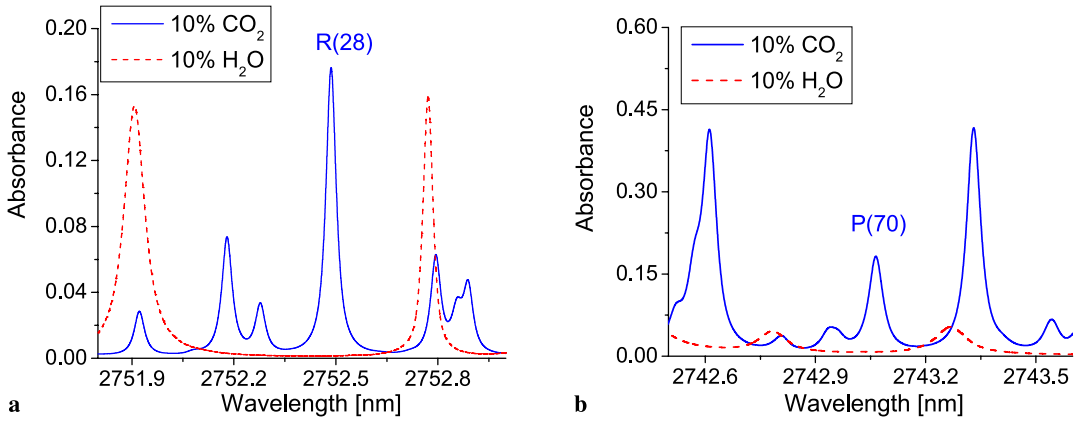

FIGURE 2 Calculated spectra of 10% CO_2 and 10% H_2O under combustion conditions: $T = 1500$ K, $P = 1$ atm, $L = 10$ cm. **a** The $R(28)$ transition of the $\nu_1 + \nu_3$ band at 2752.48 nm (3633.08 cm^{-1}) has lower-state energy (E'') of 316.77 cm^{-1}; **b** the $P(70)$ transition of the $\nu_1 + \nu_3$ band at 2743.06 nm (3645.56 cm^{-1}) has an E'' of 1936.09 cm^{-1}

band is selected because of its large line-strength and freedom from interference of neighboring CO_2 and H_2O transitions, as shown in Fig. 2a. The large line-strength of this transition combined with a relatively low value of lower-state energy ($E'' = 316.77\ cm^{-1}$) enables measurements over a wide range of temperatures (300–2000 K). To make temperature measurements in hot combustion gases, a second CO_2 line is selected that has a relatively high lower-state energy ($E'' = 1936.09\ cm^{-1}$). The $P(70)$ transition of the $\nu_1 + \nu_3$ vibrational band is also well isolated from neighboring transitions, as shown in Fig. 2b. To characterize the performance of this two-line temperature sensor, the line-strength ratio, R, of the two transitions is plotted in Fig. 3 as a function of temperature along with the sensitivity of this line pair for temperature measurements. Typically, the line-strength ratio should not be too far from unity. The sensitivity, defined here as the unit change in the normalized ratio, $\Delta R/R$, for a unit change in the normalized temperature, $\Delta T/T$, should be at least 1 for temperature measurements with small uncertainty. Line-strength ratio and sensitivity curves suggest that this line pair can be used for accurate temperature measurements between 800 and 2000 K.

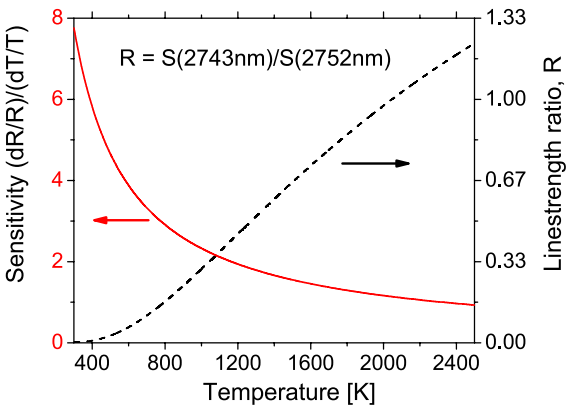

FIGURE 3 Ratio of line-strengths of 2743- and 2752-nm lines is shown on the *right-hand axis* while the temperature sensitivity is shown on the *left-hand axis*

4 Spectroscopic results

Accurate measurements of fundamental spectroscopic parameters such as line-strength and line-broadening parameters are essential in the development of new sensors for combustion environments. The collisional broadening of probed transitions increases linearly with pressure and will result in overlapping of neighboring transitions at elevated pressures. Moreover, the line-strength and broadening (and thus the overlap) change with temperature. Therefore, it is essential to study these parameters for selected transitions as a function of temperature and pressure.

These spectroscopic parameters help establish a database that is crucial to a fixed-wavelength absorption sensor where the measured absorbance is compared with the simulated absorbance from the database to infer gas properties like mole fraction and temperature.

4.1 *Experimental details*

Absorption measurements of CO_2 in a heated static cell are used to establish the needed spectroscopic data; the arrangement of the experiment is shown in Fig. 4. The DFB laser produces ∼ 2 mW of stable output power near 2.7 μm. Laser intensity and wavelength are varied by a combination of temperature and injection current using commercial controllers (ILX Lightwave LDT-5910B and LDX-3620), and the wavelength is scanned with a linear ramp of current from a function generator. Wavelength tuning with temperature and current is measured to be 0.376 $cm^{-1}/°C$ and 0.038 cm^{-1}/mA, respectively. The intensity noise of the laser is measured to be approximately 0.02% rms with a 1-MHz bandwidth. An important contribution to the measured noise is the current noise of the controller. The laser beam is transmitted through a three-section optical cell by a collimating parabolic mirror and the signal is collected by a liquid-nitrogen-cooled In–Sb detector (IR Associates IS-2.0, 1 MHz). The cell is mounted with CaF_2 windows that are wedged at 3° angle to avoid unwanted interference fringes. The cell is placed inside a heated furnace; the 9.9-cm center section of the cell is filled with test gas and located in the uniform-temperature region of the furnace, while the two

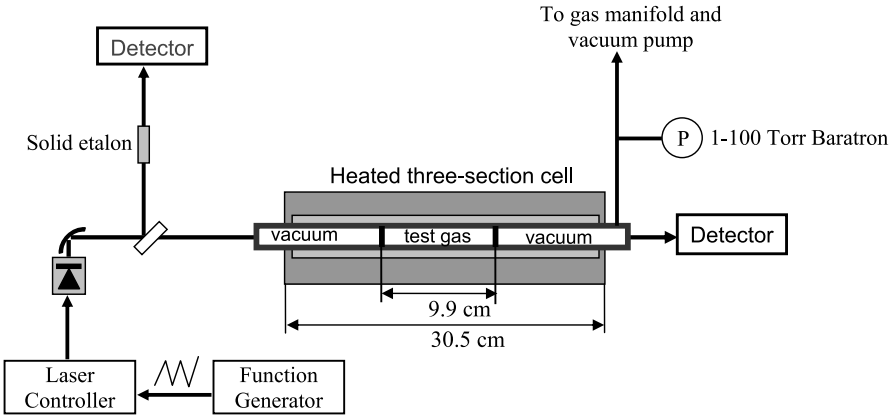

FIGURE 4 Schematic diagram of the experimental setup for the measurement of spectroscopic parameters of CO_2 transitions at a range of temperatures and pressures

outer sections are evacuated to avoid any interference by ambient CO_2 and avoid any temperature gradients near the ends of the tube furnace. Further, the optics and detector are enclosed by plastic bags purged by dry N_2 to avoid absorption interference from the ambient gases. Three type-K thermocouples (Omega) are equally spaced along the center section of the heated cell to determine the temperature of gas samples; the maximum temperature difference observed between the thermocouples is $< 1\%$. Cell pressure is measured by a 100-Torr capacitance manometer (MKS 620A) with an accuracy of $\pm 0.12\%$ of reading. A solid germanium etalon (FSR $= 0.016\,\mathrm{cm}^{-1}$) is used to measure the wavelength tuning, while the absolute wavelength is calibrated by the well-known positions of the strong CO_2 transitions.

The laser wavelength was measured using a free-space mid-IR wavelength meter (Bristol 621). This measurement, combined with relative measurements using a solid etalon, provided absolute line positions which are in excellent agreement with the HITRAN database. The HITRAN line-center values are more precise than our measurements and are used here. The laser wavelength is tuned over a range of about $1\,\mathrm{cm}^{-1}$ at a frequency of 1 kHz, while the detector (1-MHz bandwidth) signals are sampled at 10 MHz. Any background signal (e.g. detector offset, thermal emission) is subtracted from the transmitted laser intensity I_t. The baseline laser intensity I_0 is inferred by fitting the part of the scan without absorption with a third-order polynomial. The spectral absorbance is then calculated using (3) and the line shape of the target transition is best fitted using a Voigt profile. The Voigt profile is calculated using numerical approximation [18] and is least-square fitted to the measured absorbance using a nonlinear Levenberg–Marquardt algorithm.

4.2 *Measurement of line-strength*

Representative data for the CO_2 transition at $\nu_0 = 3633.08\,\mathrm{cm}^{-1}$ (2752 nm) overlaid with a best-fit Voigt profile are shown in Fig. 5 at the experimental conditions of $T = 871$ K and $P = 20.92$ Torr. The peak-normalized residual values are less than 2% for all of the data sets, indicating that the Voigt profile adequately models the absorption line shape at these conditions.

The line-strength measurement procedure is illustrated in Fig. 6 and is similar to that used in previous spectroscopic studies [19]. At specific temperature and pressure, the measured absorbance is fitted to a Voigt line shape, and the integrated absorbance is calculated from the best-fit Voigt values. At each pressure, 10 measurements are made, and the average of the integrated absorbance values is determined. Figure 6a illustrates the variation of the average integrated absorbance with pressure at 722 K for the 2752-nm line. Following (4), the line-strength at this temperature is inferred from the slope of the linear fit to the data in Fig. 6a. The measured line-strength at 11 different temperatures between 296 K and 1200 K is plotted in Fig. 6b. These measured data are fitted to (7) with E'' and $S(296\,\mathrm{K})$ as free parameters. The good agreement (within 2%) between the fitted value of E'' and the HITRAN 2004 value confirms the spectroscopic assignment in HITRAN. The lower-state energy is fixed at the HITRAN 2004 value, as the E'' values listed in HITRAN are considered to be quite accurate. The line-strength at the reference temperature $S(296\,\mathrm{K})$ is then obtained from a one-parameter best fit and has an uncertainty of 2%. The tabulated line-strength from HITRAN 2004 is also shown in Fig. 6b for comparison.

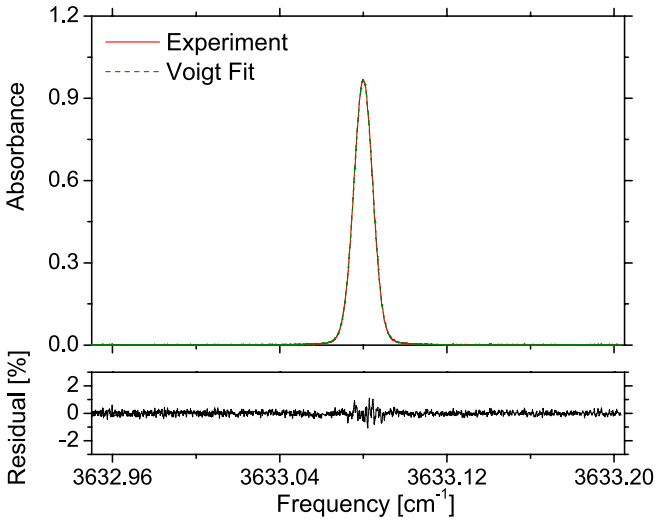

FIGURE 5 Single-scan absorption data taken at 1 kHz with pure CO_2 for the $R(28)$ transition at $P = 4.96$ Torr, $T = 655.2$ K, and $L = 9.9$ cm. Shown at the *top* is the best-fit Voigt profile to the experimental data. The peak-absorbance normalized residual (experiment – Voigt) is shown at the *bottom*

Following the same procedure described above, the line-strength of the second CO_2 transition near 2743 nm is measured as a function of temperature and plotted in Fig. 7. Table 1 compares the measured line-strength values for these transi-

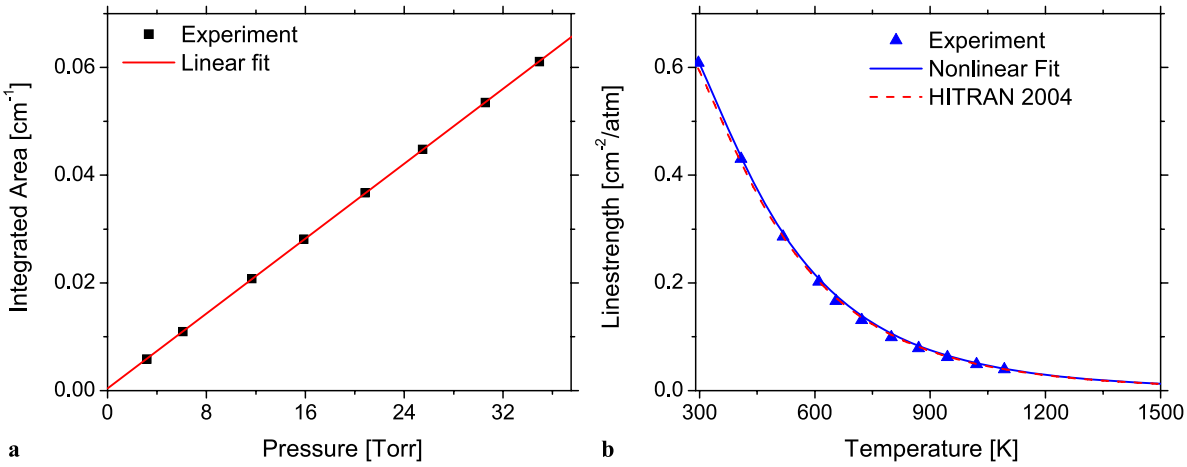

FIGURE 6 Line-strength measurements for the CO_2 transition near 3633.08 cm^{-1}: **a** the measured integrated absorbance versus CO_2 pressure at $T = 722$ K, and the linear fit used to infer the line-strength; **b** the measured line-strength versus temperature and the one-parameter best fit to infer the line-strength at reference temperature $S(296\,\text{K}) = 0.613 \pm 0.012$ cm^{-2}/atm

Species	υ_0 [cm^{-1}]	E'' [cm^{-1}]	S(296 K)		γ_{self}(296 K) [cm^{-1}/atm]		n	γ_{CO_2-Ar}(296 K) [cm^{-1}/atm]	m
			Measured	HITRAN04	Measured	HITRAN04	Measured	Measured	Measured
CO_2	3633.08	316.77	6.13×10^{-1} (2%)	5.98×10^{-1} (2%–5%)	0.171 (2.5%)	0.177 (2%–5%)	0.654 (2.2%)	0.112 (2.7%)	0.658 (2.6%)
CO_2	3645.56	1936.09	7.04×10^{-4} (2%)	7.12×10^{-4} (2%–5%)	0.130 (2.5%)	0.124 (2%–5%)	0.695 (3.3%)	0.091 (2.9%)	0.694 (2.9%)

TABLE 1 Line-strengths and broadening parameters for the two selected CO_2 transitions. Measured values are compared with HITRAN 2004 values wherever available. Uncertainties are given in the parentheses

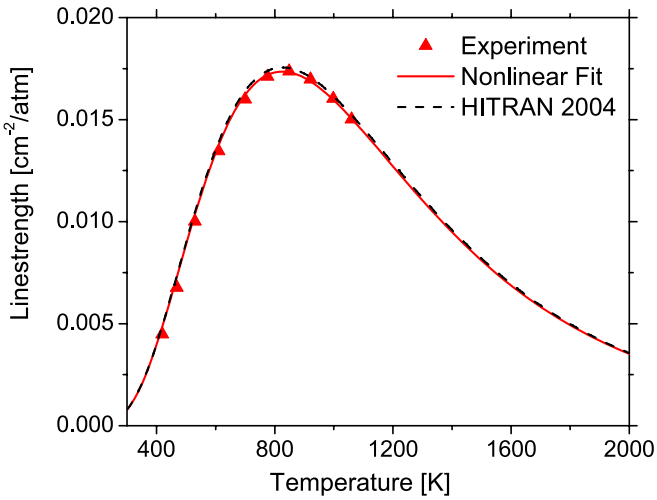

FIGURE 7 Measured line-strength versus temperature for the CO_2 transition near 3645.56 cm^{-1} and the one-parameter best fit to infer the line-strength at reference temperature $S(296\,\text{K}) = 7.04 \times 10^{-4} \pm 1.41 \times 10^{-5}$ cm^{-2}/atm

tions near 3633.08 cm^{-1} and 3645.56 cm^{-1} with the values in the HITRAN database.

4.3 *Measurement of self-broadening and Ar-broadening coefficients*

The collisional FWHM is obtained from the Voigt fit of the measured profile. At a given temperature, the collisional FWHM values at various pressures of pure gas (CO_2) are fitted to a straight line to infer the self-broadening coefficient, as shown in Fig. 8a for the 2752-nm line. The self-broadening coefficient at the reference temperature, $2\gamma_{self}(296\,\text{K})$, and its temperature exponent n are then calculated from a two-parameter best fit of the measured $2\gamma_{self}$ at various temperatures according to (6), as illustrated by Fig. 8b. Following a similar procedure, the self-broadening coefficient $2\gamma_{self}$ for the 2743-nm CO_2 line is plotted in Fig. 9. The measured results are also compared with values in the HITRAN 2004 database in Table 1.

Collisional broadening of CO_2 transitions by argon is measured in a manner analogous to self-broadening measurements except that the probed gas mixture comprises 10% CO_2 in argon. Figure 10 plots the Ar-broadened CO_2 line shape near 3633.08 cm^{-1} ($P = 359$ Torr, $T = 931$ K, 10% CO_2 in Ar) overlaid with the best-fit Voigt profile. Collisional FWHM is measured as the pressure is varied from 50 to 700 Torr and the Ar-broadening coefficient ($2\gamma_{CO_2-Ar}$) is obtained after subtracting the contribution from self-broadening. Figure 11 plots $2\gamma_{CO_2-Ar}$ as a function of temperature for the two CO_2 transitions near 3633.08 and 3645.56 cm^{-1}. The uncertainties of our measured line-strength and broadening coefficients have contributions from the uncertainties in temperature (1%), gas pressure (0.12%), path length (0.5%), and statistical errors in the baseline and Voigt profile fits (1%).

5 Sensor validations

The fixed-wavelength TDL absorption sensor is first validated in the heated static cell and shock-tube before

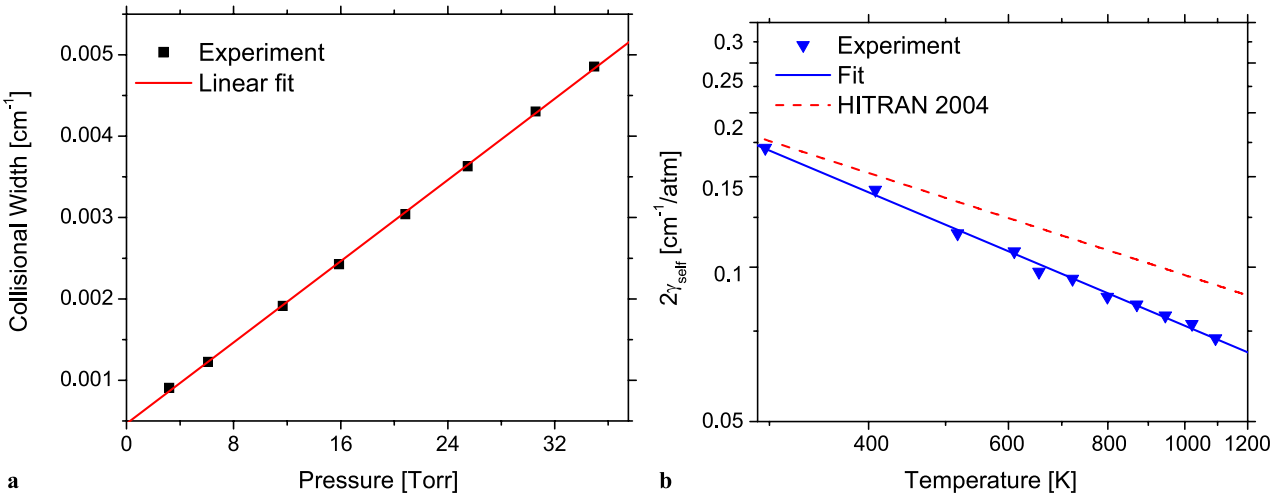

FIGURE 8 Self-broadening coefficient measurements for the CO_2 transition near 3633.08 cm^{-1}: **a** the measured collisional FWHM versus pressure at $T = 722$ K, and the linear fit to infer $2\gamma_{self}$; **b** the measured $2\gamma_{self}$ versus temperature, and the two-parameter best fit to infer $2\gamma_{self}(296\,\text{K}) = 0.171 \pm 0.004$ cm^{-1}/atm and $n = 0.654 \pm 0.014$. The HITRAN $2\gamma_{self}$ is also plotted for comparison with a typical value of $n = 0.50$

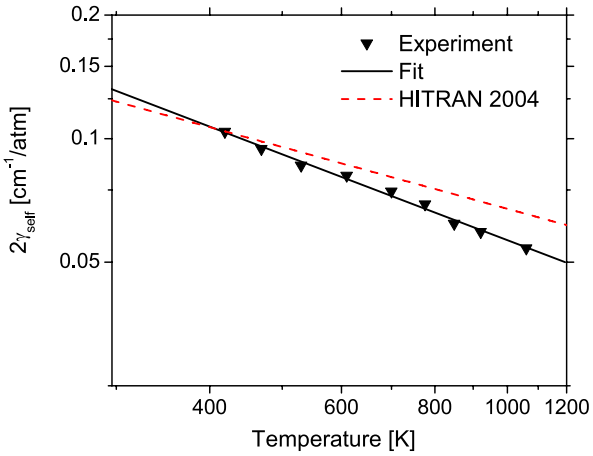

FIGURE 9 Measured self-broadening coefficient $2\gamma_{self}$ versus temperature for the CO_2 transition near 3645.56 cm^{-1}, and the two-parameter best fit to infer $2\gamma_{self}(296\,\text{K}) = 0.130 \pm 0.003$ cm^{-1}/atm and $n = 0.695 \pm 0.023$. The HITRAN $2\gamma_{self}$ is also plotted for comparison with a typical value of $n = 0.50$

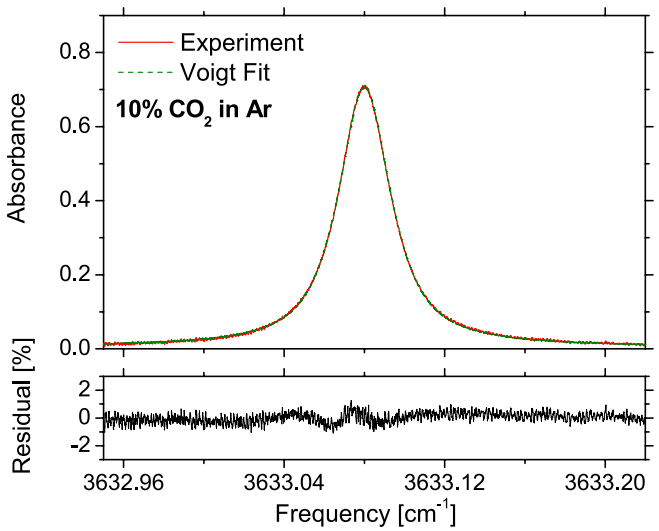

FIGURE 10 Single-scan absorption data taken at 1 kHz with 10% CO_2 in Ar for the $R(28)$ transition at $P = 359$ Torr, $T = 931$ K, and $L = 9.9$ cm. Shown at the *top* is the best-fit Voigt profile to the experimental data. The residual of the fit is shown at the *bottom*

being used in combustion applications. The laser wavelength is fixed by operating the laser at constant current and temperature. Cell measurements show that the laser can be reproducibly tuned to line center for the same set values of injection current and temperature, suggesting that the 2.7-μm device and the low-noise controllers provide stable and reproducible laser wavelength. The bandwidth of these fixed-wavelength measurements is limited by the detector bandwidth, which in this case is 1 MHz.

5.1 *Static cell*

For static cell validations, an arrangement similar to that shown in Fig. 4 is used where one of the two CO_2 laser beams is transmitted through the cell by using a flipper mirror. The laser wavelengths are fixed at the line centers of the two probed transitions ($R(28)$ and $P(70)$). The heated static cell is evacuated before each experiment to record the baseline laser intensity I_0 for both lasers. The cell is then filled with CO_2–Ar mixture to $P \sim 1$ atm, and the transmitted laser intensity I_t is recorded for each laser. Measured absorbance ($-\ln(I_t/I_0)$) values are compared with simulation to infer gas temperature and CO_2 concentration in the cell. The top panel of Fig. 12 compares the thermocouple measurements with the temperatures from the fixed-wavelength CO_2 sensor. The temperatures determined from the TDL sensor are in good agreement with the thermocouple readings over the entire temperature range (400–1100 K). The bottom panel of Fig. 12 shows the ratio of the CO_2 mole fraction measured by the TDL sensor and the known mixture mole fraction. The standard deviation between the measured and known values is 1.8% for temperature and 1.6% for CO_2 mole fraction. The excellent agreement between the measured and actual values confirms the accuracy of the TDL sensor for temperature and CO_2 concentration measurements.

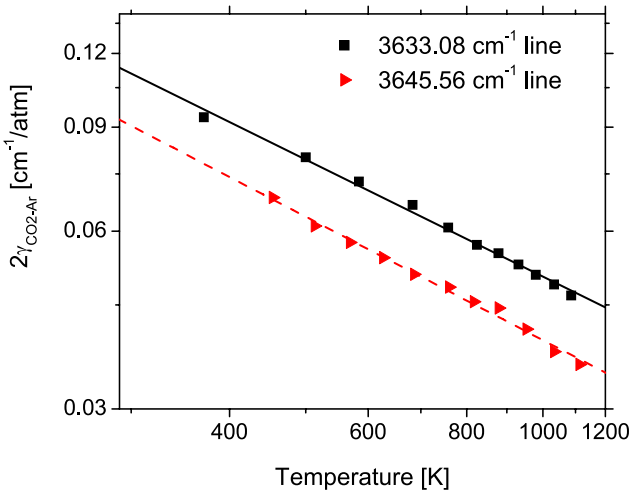

FIGURE 11 Measured Ar-broadening coefficient $2\gamma_{CO_2-Ar}$ versus temperature for the two CO_2 transitions. The two-parameter best fit gives $2\gamma_{CO_2-Ar}(296\,K) = 0.1123 \pm 0.003\,cm^{-1}/atm$ and $m = 0.658 \pm 0.017$ for the $R(28)$ transition near 3633.08 cm^{-1}, while for the $P(70)$ transition near 3645.56 cm^{-1} the fit gives $2\gamma_{CO_2-Ar}(296\,K) = 0.091 \pm 0.0027\,cm^{-1}/atm$ and $m = 0.694 \pm 0.02$

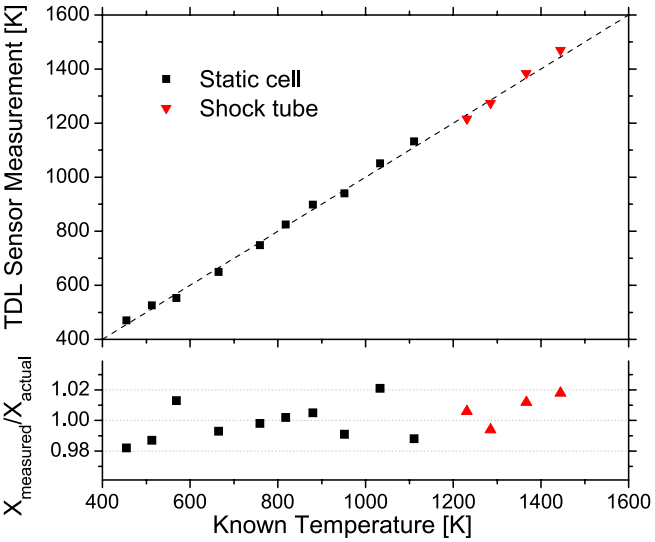

FIGURE 12 Validation measurements of the fixed-wavelength direct-absorption CO_2 sensor. The first 10 points represent the validation experiments carried out in the well-controlled static cell ($P \sim 1$ atm, 10% CO_2 in Ar, $L = 9.9$ cm). The last four points represent the validation experiments carried out in the shock-tube ($P_5 \sim 1.3$ atm, 5% CO_2 in Ar, $L = 14.13$ cm)

5.2 *Shock-tube*

To validate the sensor accuracy and response at combustion temperatures, experiments are conducted in shock-heated CO_2–Ar mixtures behind reflected shock waves in a helium-pressure-driven stainless-steel shock-tube. The driven section is 8.54-m long and the driver section 3.35-m long; both sections have an inner diameter of 14.13 cm. Further details of the shock-tube setup can be found elsewhere [20, 21]. The maximum CO_2 mole fraction is 5% for all our shock-tube measurements and the largest peak absorbance is 0.36 for the measurements in shock-heated gases. TDL measurements are made at a location 2 cm from the end wall. Figure 13 is a schematic of the experimental setup showing

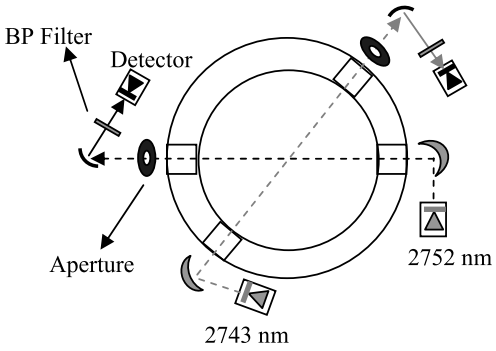

FIGURE 13 Experimental setup for shock-tube measurements with the fixed-wavelength CO_2 sensor

cross-section of the shock-tube and optical arrangement. The light from each laser is collimated and transmitted through different windows on the shock-tube side wall. The optical configuration is based on the assumption that the gas properties across the shock-tube are uniform. Since the typical test times of interest in shock-tube experiments are on the order of 10 μs–2 ms, fast ($\sim$ 1 MHz) time response is needed for measurements of CO_2 concentration and temperature, and the fixed-wavelength approach is used here.

The test procedure is similar to the one described for static cell validations. Prior to each experiment, the shock-tube is evacuated to record the baseline intensity I_0 for each laser. The shock-tube is then filled with CO_2–Ar mixture to $P_1 = 30$–50 Torr. The data-acquisition system is triggered by the pressure transducer to record the pressure and transmission signals (I_t) for both CO_2 lasers during the shock-heating process. The time histories of gas temperature and CO_2 concentration are then inferred by comparing the measured absorbance with simulation. Figure 14 plots the measured time history of pressure and temperature during a shock with initial 5% CO_2/Ar mixture at $P_1 = 39.8$ Torr and $T_1 = 297$ K. The average measured temperature over the time interval 0–1 ms is 1274 K (standard deviation = 1%). This is in excellent agreement with the value calculated from the ideal shock

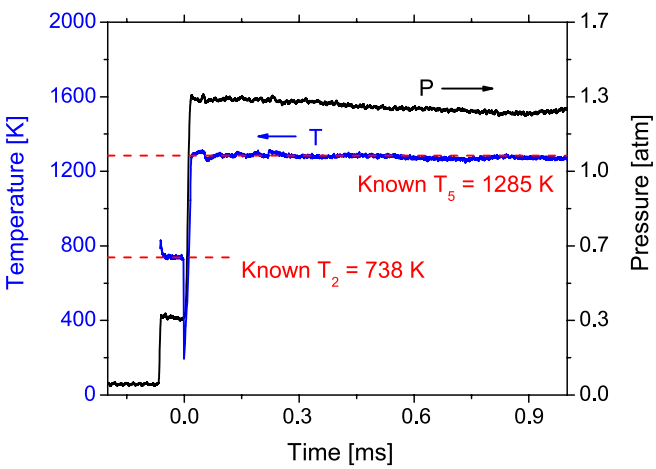

FIGURE 14 Measured temperature and pressure trace during a shock with 5% CO_2–Ar mixture. Initial conditions: $P_1 = 39.8$ Torr and $T_1 = 297$ K; incident shock conditions (calculated): $P_2 = 0.352$ atm and $T_2 = 738$ K; reflected shock conditions (calculated): $P_5 = 1.314$ atm and $T_5 = 1285$ K

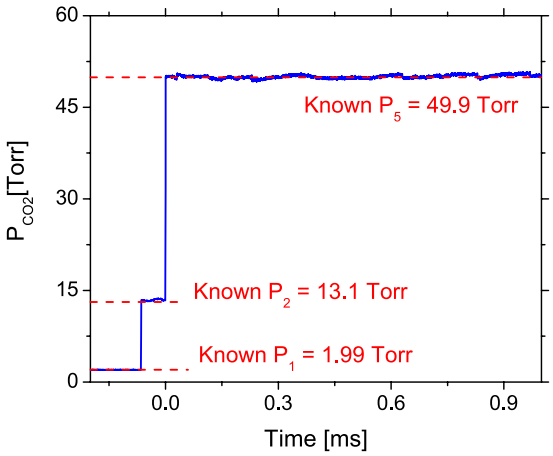

FIGURE 15 Measured CO_2 partial pressure by the fixed-wavelength sensor during the same shock as Fig. 14 (5% CO_2–Ar mixture)

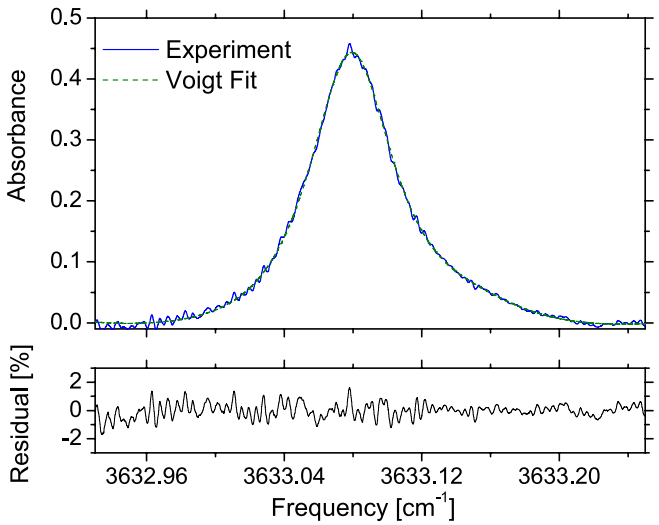

FIGURE 16 Single-scan absorption data taken at 1 kHz for concentration measurement in a flat-flame burner with the CO_2 transition near 3633.08 cm^{-1} at $T = 1495$ K, $P = 1$ atm, $L = 25.4$ cm, equivalence ratio $\Phi = 0.98$. Shown at the *top* is the best-fit Voigt profile to the experimental data, while the residual of the fit is shown at the *bottom*. Measured mole fraction is $12.52\% \pm 0.43\%$

equations, $T_5 = 1285$ K. CO_2 mole fraction can be computed using the measured pressure, temperature, and transmission signal of either laser. The measured mole fraction is multiplied with the pressure trace and the resulting partial pressure of CO_2 is shown in Fig. 15. The relatively low E'' of the 2752-nm transition allows accurate absorption measurements in the pre-shock mixture, whereas both lasers have good absorption signals behind the incident and reflected shocks. CO_2 mole fractions obtained from the two lasers are in good agreement with each other (within 0.8%).

Similar tests are performed at different temperatures by varying the initial fill pressure (P_1). The results are plotted in Fig. 12 where the top panel compares the measured sensor temperature with that calculated from ideal shock relations (T_5) and the bottom panel compares the measured CO_2 mole fraction with known mixture values. The measured and calculated temperatures are in good agreement (within 1.4%) over the tested temperature range 1200–1500 K and the measured mole fraction agrees with the mixture values within 1.5%. These results validate the sensor accuracy and response for temperature and CO_2 concentration measurements at combustion temperatures and illustrate the potential for applications in combustion studies with varying temperatures and mole fractions.

6 Combustion applications

6.1 *Flat-flame burner measurements*

CO_2 absorption measurements are made in the burned gases above a flat-flame burner. The 25.4-cm-long burner, operated on premixed ethylene (C_2H_4) and air, provides a relatively uniform temperature distribution to within 4% as measured by a type S thermocouple traversed along the laser path. The flows of ethylene and air are metered with calibrated rotameters. Varying the fuel and/or air flow rates produces a range of equivalence ratios of $\Phi = 0.6$–1.4. Uncertainty in the fuel/air flow rates, and thus the equivalence ratio, is approximately 3%. The thermocouple temperature is corrected by approximately +50 K for radiation effects [22].

Large sensor bandwidth is not required in these measurements as the flame conditions remain quite stable. Therefore, the 2752-nm laser is tuned over the $R(28)$ transition by modulating its current at 1 kHz and the measured profile is fitted with a Voigt line shape to determine the integrated absorbance. The mole fraction of absorbing species is then obtained from (2) using radiation-corrected thermocouple data for temperature. Background thermal emission signals (< 3% of the laser intensity) were subtracted from the transmission data before analysis of absorption spectra. Figure 16 shows the measured absorption line shape fitted with the Voigt function at the flame conditions to deduce CO_2 mole fraction from the integrated absorbance.

The measured CO_2 concentrations are compared with chemical equilibrium calculations and found to be in very good agreement. Figure 17 shows CO_2 measurements carried out at different fuel–air equivalence ratios compared with equilibrium values at the measured temperature. Two points have error bars representing the typical uncertainty estimate

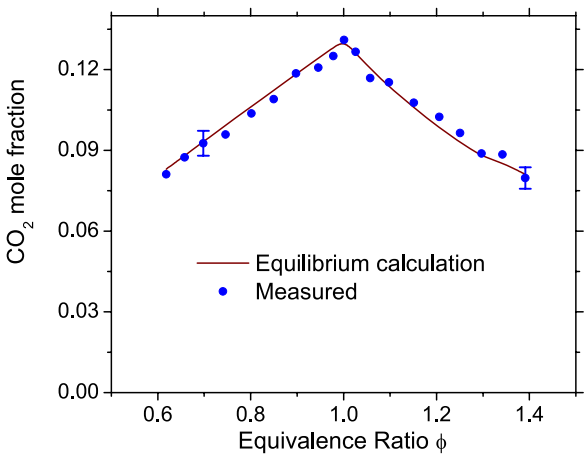

FIGURE 17 Comparison of measured CO_2 mole fractions in the exhaust gases above a flat-flame burner with chemical equilibrium calculations. The *error bars* represent the uncertainty in the measured concentrations

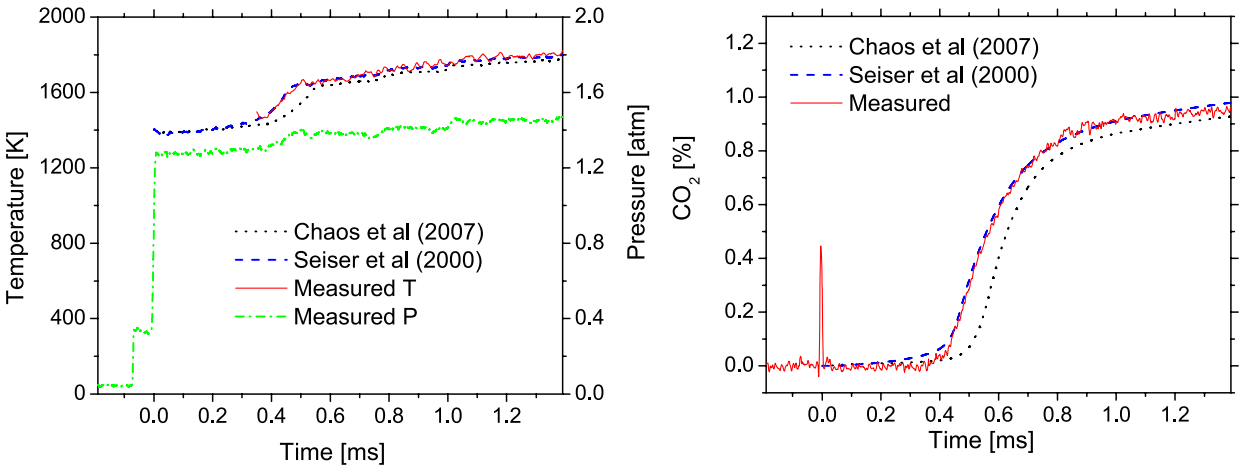

FIGURE 18 Measured temperature T and CO_2 concentration during a shock with initial mixture: 0.2% heptane/2.2% O_2/Ar; simulations using two kinetic mechanisms are shown. $P_1 = 35.1$ Torr, $T_1 = 297$ K; $P_2 = 0.335$ atm, $T_2 = 786$ K; $P_5 = 1.275$ atm, $T_5 = 1404$ K

for measured concentrations in fuel-lean and -rich conditions. The high absorbance levels obtained in these measurements reflect the advantage of using strong transitions near the 2.7-μm region, thereby offering better sensitivity and signal-to-noise ratio than obtained with transitions at shorter wavelengths.

The Equilibriumcalculations are dependent on the measured equivalence ratio and the measured flame temperature. These measurements have uncertainties of 3% and 2%, respectively. Uncertainty in the measured mole fraction accounts for the uncertainty in line-strength (2%), uncertainty in temperature measurement (2%), and errors associated with baseline and Voigt profile fit (1%). We estimate 0.1% minimum detectable absorbance at 1 kHz, which corresponds to a detection limit of 9 ppm per meter at 1000 K and 1 atm for the CO_2 transition at 3633.08 cm^{-1}. For this low-E'' line, the detection limit at 296 K and 1 atm would be 1.8 ppm per meter.

Note that scanned-wavelength direct absorption does not require knowledge of accurate broadening parameters and line center, but the laser scan rate limits the time response. For the approximately 0.35-cm^{-1} scanning range needed for atmospheric pressure measurements, bandwidth is limited to roughly 25 kHz for the DFB lasers used here. A high-bandwidth fixed-wavelength scheme is therefore used for our time-resolved measurements of shock-heated gases.

6.2 *Shock-tube kinetic measurements*

Shock-tubes are commonly used to study gas phase combustion reactions under a wide range of temperatures and pressures that are difficult to obtain in other types of testing facilities. By measuring the formation and depletion of key combustion species produced in the reaction zone behind reflected shock waves, kinetic reaction rates and characteristic times can be obtained [23–27]. The accurate measurement of combustion species in shock-tubes is therefore critical, and non-intrusive optical diagnostic techniques such as laser absorption and infrared emission are commonly employed.

Here, a fixed-wavelength CO_2 temperature sensor is used in a demonstration kinetic study of heptane–O_2 ignition. The bandwidth is $\sim$ 1 MHz, and the experimental setup is similar to that shown in Fig. 12. The measured temperature and CO_2 mole fraction are plotted in Fig. 18 for a shock with 0.2% heptane and 2.2% O_2 in Ar (equivalence ratio $\Phi = 1$) as the initial mixture. The measurement results are compared with simulations using (1) the Chaos et al. detailed kinetics mechanism [28] and (2) the Seiser et al. mechanism [29]. The simulations are performed using CHEMKIN in conjunction with a simple reactive gas dynamics model [30]. The measured temperature and concentration are both in good agreement with Seiser's mechanism. Measurements of CO_2 profile and temperature can be made for a variety of fuels and hydrocarbons, and we expect that such data can greatly aid the validation of existing kinetic mechanisms and for developing more accurate mechanisms.

7 Summary

Tunable diode-laser absorption measurements of CO_2 transitions near 2.7 μm are reported. High-temperature absorption spectra of CO_2 and H_2O were simulated with HITRAN to find suitable CO_2 transitions for in situ combustion monitoring. The two selected transitions, $R(28)$ and $P(70)$, belonging to the $\nu_1 + \nu_3$ vibrational band, have appreciably different lower-state energies for sensitivity of temperature measurements, and are free of interference absorption from H_2O. Pertinent spectroscopic parameters for these transitions were measured in a heated static cell and compared with literature values. A fixed-wavelength direct-absorption CO_2 temperature sensor was validated in a static cell and shock-tube for accurate measurements of gas temperature and CO_2 concentration with 1-MHz bandwidth. Wavelength-scanned absorption measurements of CO_2 concentration in the burned gases of a flat-flame burner at atmospheric pressure were then made with a 1-kHz bandwidth to demonstrate the capability for in situ monitoring by use of these diode-laser sensors. The sensor was then applied to heptane ignition experiments for measurements of CO_2 concentration and temperature to illustrate the usefulness of this sensor for chemical kinetic studies in shock-heated gases. Taken with our earlier presentation of preliminary results [14], the data presented here are the first TDL absorption measurements of combustion prod-

ucts using transitions in the 2.7-μm region. The increased absorption strength of transitions in this wavelength region offer opportunities for more sensitive and accurate combustion measurements, and shorter path lengths, than previous absorption work using CO_2 bands at shorter wavelengths.

ACKNOWLEDGEMENTS We gratefully acknowledge support from the Air Force Office of Scientific Research (AFOSR) with Dr. Julian Tishkoff as technical monitor, and the Army Research Office (ARO) with Dr. Ralph Anthenien as technical monitor.

REFERENCES

1 M.G. Allen, Meas. Sci. Technol. **9**, 545 (1998)
2 J.A. Silver, D.J. Kane, P.S. Greenberg, Appl. Opt. **34**, 2787 (1995)
3 H. Teichert, T. Fernholz, V. Ebert, Appl. Opt. **42**, 2043 (2003)
4 R.K. Hanson, J.B. Jeffries, in *25th AIAA Aerodynamic Measurement Technology and Ground Testing Conference*, Washington, DC (2006), AIAA-2006-3441
5 D. Richter, D.G. Lancaster, F.K. Tittle, Appl. Opt. **39**, 4444 (2000)
6 L.S. Rothman, D. Jacquemart, The 2004 edition of the HITRAN compilation, in *8th HITRAN Database Conference* (Harvard-Smithsonian Center for Astrophysics, Boston, MA, 2004), p. 26
7 HITRAN web site, http://cfa-www.harvard.edu/HITRAN/
8 D.M. Sonnenfroh, M.G. Allen, Appl. Opt. **36**, 3298 (1997)
9 R.M. Mihalcea, D.S. Baer, R.K. Hanson, Appl. Opt. **36**, 8745 (1997)
10 R.M. Mihalcea, D.S. Baer, R.K. Hanson, Meas. Sci. Technol. **9**, 327 (1998)
11 M.E. Webber, S. Kim, S.T. Sanders, D.S. Baer, R.K. Hanson, Y. Ikeda, Appl. Opt. **40**, 821 (2001)
12 R.M. Mihalcea, D.S. Baer, R.K. Hanson, Appl. Opt. **37**, 8341 (1998)
13 Nanosystems and Technologies GmbH, http://www.nanoplus.com
14 A. Farooq, H. Li, J.B. Jeffries, R.K. Hanson, in *AIAA 43rd Joint Propulsion Conference*, Washington, DC (2007), AIAA-2007-5015
15 D.S. Baer, V. Nagali, E.R. Furlong, R.K. Hanson, M.E. Newfield, AIAA J. **34**, 489 (1996)
16 V. Nagali, S.I. Chou, D.S. Baer, R.K. Hanson, Appl. Opt. **35**, 4026 (1996)
17 A. Goldman, R.R. Gamache, A. Perrin, J.M. Flaud, C.P. Rinsland, L.S. Rothman, J. Quant. Spectrosc. Radiat. Transf. **66**, 455 (2000)
18 E.E. Whiting, J. Quant. Spectrosc. Radiat. Transf. **16**, 611 (1976)
19 X. Liu, J.B. Jeffries, R.K. Hanson, K.M. Hinckley, M.A. Woodmansee, Appl. Phys. B **82**, 469 (2006)
20 M.A. Oehlschlaeger, D.F. Davidson, R.K. Hanson, J. Phys. Chem. A **108**, 4247 (2004)
21 J.T. Herbon, R.K. Hanson, D.M. Golden, C.T. Bowman, Proc. Combust. Inst. **29**, 1201 (2002)
22 C.R. Shaddix, Proc. Natl. Heat Transfer Conf. **33**, 282 (1999)
23 I. Glassman, *Combustion* (Academic, San Diego, CA, 1996)
24 C.T. Bowman, R.K. Hanson, J. Phys. Chem. **83**, 757 (1979)
25 R.K. Hanson, D.F. Davidson, in *Handbook of Shock Waves*, vol. 1, ed. by G. Ben-Dor, O. Igra, T. Elperin (Academic, San Diego, CA, 2001), Chap. 5.2
26 H.J. Curran, P. Gaffuri, W.J. Pitz, C.K. Westbrook, Combust. Flame **114**, 149 (1998)
27 D.F. Davidson, R.K. Hanson, Int. J. Chem. Kinet. **36**, 510 (2004)
28 M. Chaos, A. Kazakov, Z. Zhao, F.L. Dryer, Int. J. Chem. Kinet. **39**, 399 (2007)
29 R. Seiser, H. Pitsch, K. Seshadri, W.J. Pitz, H.J. Curran, Proc. Combust. Inst. **28**, 2029 (2000)
30 H. Li, Z.C. Owens, D.F. Davidson, R.K. Hanson, Int. J. Chem. Kinet., in press